



CrossMark
click for updates

Cite this: *RSC Adv.*, 2016, 6, 68515

Reactivity of different surface sites with silicon chlorides during atomic layer deposition of silicon nitride†

Luchana L. Yusup,^a Jae-Min Park,^a Yong-Ho Noh,^a Sun-Jae Kim,^a Won-Jun Lee,^{*a} Sora Park^{‡b} and Young-Kyun Kwon^{*b}

We studied the reactivity of different surface sites of β - Si_3N_4 with silicon chlorides during the first half reaction of an atomic layer deposition (ALD) process using *ab initio* density functional theory calculations to understand the underlying reaction mechanism. We considered three types of surface sites, NH^*/SiH^* , $\text{NH}^*/\text{SiNH}_2^*$, and under-coordinated bare >Si=N- . The reactions of the silicon chlorides with $\text{NH}^*/\text{SiNH}_2^*$ and >Si=N- are energetically favorable, whereas the reactions are endothermic with NH^*/SiH^* . On >Si=N- , the silicon and chlorine atoms of the precursors easily react with the unsaturated nitrogen and silicon atoms, respectively, resulting in very low energy barriers for the reaction. However, on NH^*/SiH^* and $\text{NH}^*/\text{SiNH}_2^*$, the reaction undergoes high energy barriers due to the dissociation of a hydrogen atom from the surface or a chlorine atom from the precursor. We further found that Si_2Cl_6 shows energies of reaction lower than those of SiCl_4 on >Si=N- . By discovering the influence of surface reaction sites on ALD reactions, we designed a new 3-step ALD process to obtain the most effective surface sites for the first half reaction, and confirmed this with deposition experiments. The N_2 plasma steps, prior to the introduction of a silicon precursor, reduced the saturation dose of Si_2Cl_6 from 10^7 L to $<10^6$ L and increased the growth rate from 0.59 Å per cycle to 1.1 Å per cycle, which agrees with our calculations. These results show that the reactivity of the surface sites plays a very important role to determine the thermodynamics and kinetics of ALD processes.

Received 27th April 2016

Accepted 4th July 2016

DOI: 10.1039/c6ra10909h

www.rsc.org/advances

1. Introduction

Silicon nitride thin films have been widely used in metal-oxide-semiconductor field-effect-transistor (MOSFET) devices due to their chemical stability and resistance to diffusion of impurities.^{1–3} Silicon nitride thin films can be grown using several deposition methods, such as low-pressure chemical vapor deposition (LPCVD), plasma-enhanced CVD (PECVD), and atomic layer deposition (ALD).^{4–20} Among them, ALD is the most promising method to obtain silicon nitride thin films with excellent quality and high conformality *via* a low temperature deposition process, which is critical especially in high quality gate spacer applications.^{2,3}

In the production of silicon nitride films for the microelectronics industry, silicon chlorides combined with ammonia

have most widely been used as precursors and reactants.²¹ Silicon chloride precursors attract vast interest not only because of their superior performances, but also their easy synthesis owing to their simple structures. They can even be purchased inexpensively from many materials companies. For thermal ALD of silicon nitride, various silicon chlorides, such as SiCl_4 ,^{13,14} SiH_2Cl_2 ,¹⁵ or Si_2Cl_6 ,¹⁶ and ammonia (NH_3) were used, except for reports in which hydrazine (N_2H_4) was used instead of ammonia.^{22,23} The structure of silicon chloride molecules exerts a strong influence on the reaction kinetics of ALD of silicon nitride. The saturation doses of silicon precursors were reported to be 2×10^{10} ,¹⁴ 6×10^9 ,¹⁵ and 2×10^8 L (ref. 16) ($1 \text{ L} = 10^{-6}$ Torr s) for SiCl_4 , SiH_2Cl_2 , and Si_2Cl_6 , respectively. These results show that the first half reaction in the ALD of silicon nitride determines the reaction rate. Deposition temperatures are typically 400–550 °C, which is slightly higher than the requirement of next-generation CMOS devices. The plasma-enhanced ALD (PEALD) of silicon nitride using SiH_2Cl_2 and NH_3 plasma showed a low ALD process temperature below 400 °C and a low saturation dose of 5.4×10^6 L compared with those of thermal ALD. However, the silicon nitride films prepared by the PEALD method were silicon-rich and showed a low refractive index of approximately 1.6,²³ which is significantly lower than that of air-

^aDepartment of Nanotechnology and Advanced Materials Engineering, Sejong University, Seoul 05006, Korea. E-mail: wjlee@sejong.ac.kr

^bDepartment of Physics and Research Institute for Basic Sciences, Kyung Hee University, Seoul 02447, Korea. E-mail: ykkwon@khu.ac.kr

† Electronic supplementary information (ESI) available. See DOI: 10.1039/c6ra10909h

‡ Current address: ETRI (Electronics and Telecommunications Research Institute), Daejeon, 305-700, Korea.

exposed silicon nitride films prepared by thermal ALD (typically, 1.8).¹⁶

Different surface sites of silicon nitride have been constructed using different deposition processes resulting in hydrogen passivated sites^{15–17,24} or a low hydrogen content on the surface.^{11–14,18,20–24} Hydrogen-passivated sites on β - Si_3N_4 surfaces are NH^* and SiH^* (NH^*/SiH^*), where the surface species are indicated by the asterisks. On the other hand, the surface sites of NH^* and SiNH_2^* ($\text{NH}^*/\text{SiNH}_2^*$) are formed by NH_3 gas during the thermal ALD process or by NH_3 plasma during the PEALD process, which was confirmed by an Si-NH_x peak from XPS analysis,¹³ and an NH_2 peak from FTIR absorption spectra.¹⁴ Meanwhile, under-coordinated bare (>Si=N-) surface sites have also been generated by N_2 plasma during the PEALD process.²⁰

Compared to these experimental studies on the surface structures of silicon nitride, there have been only a few theoretical studies. A density functional theory (DFT) calculation showed that hydrogenated amorphous silicon nitride has Si-H and N-H sites on its surface.²⁵ Another DFT study revealed that a hydrogen atom adsorbed on an amorphous silicon nitride binds to either an Si or N atom located on its surface to saturate its dangling bond and thus be fourfold or threefold coordinated to Si or N atoms, respectively.²⁶ Native defects in hexagonal β - Si_3N_4 have been studied by using DFT calculations, showing that both N and Si being native defect centers form donor and acceptor states in the band gap^{26,27} A DFT calculation also investigated differences in the dielectric property of silicon nitride under various circumstances, such as in bulk and thin films, or in crystalline and amorphous phases.²⁸

There have been several theoretical studies on the reactions of silicon precursors with silicon nitride surfaces. The reaction of SiH_2Cl_2 and NH_3 with NH^* and SiH_2^* surface sites during thermal CVD of silicon nitride was reported. The silicon nitride surface was modeled by a cluster of ~ 50 atoms and the reaction mechanism was studied using a combination of density functional theory (DFT), transition state theory, and quantum Rice-Ramsperger-Kassel theory.²⁹ On the other hand, cluster models with 10–30 atoms were constructed and the reaction was studied using *ab initio* MP2/6-31G**.³⁰ The reaction of SiH_4 or NH_3 with Si-H* and N-H* for the cluster model of silicon nitride having 25 atoms has been studied using DFT calculations to search for the reactive surface sites to SiH_4 or NH_3 during the thermal ALD process.³¹

Recent theoretical studies about the reaction of silicon nitride with precursors are mostly focused on the reaction of aminosilane precursors on $\text{NH}^*/\text{SiNH}_2^*$ surfaces.^{32,33} The adsorption and reaction of different aminosilanes on the cluster surface models of silicon oxide and silicon nitride consisting of ~ 70 atoms were studied using DFT calculations. Periodic slabs of β - Si_3N_4 with $\text{NH}^*/\text{SiNH}_2^*$ -terminated surfaces with a (2×2) unit cell were constructed by adding H and NH_2 ligands to β - Si_3N_4 slabs consisting of 112 atoms, and the reaction mechanism of thermal ALD was studied using the DFT method.³³ Recently, it was shown that the interaction of silicene, a quasi 2-dimensional layer of silicon, with a hybrid substrate, β - Si_3N_4 (0001)/Si (111) induces an electron transfer, which can be

modulated by the doping of the substrate. They calculated the energy of the interface model of the substrate system with and without full hydrogenation of the surface. It was computed that the bare surface is more reactive than the hydrogenated one.³⁴

In the earlier studies mentioned above, only one type of reactive sites on silicon nitride surfaces were considered to study the reaction mechanism of CVD or ALD processes. No comparative studies have been done yet on how different surface sites react with silicon precursors. Moreover, most studies were done with only a limited number of atoms up to those in a 4-layered (2×2) unit cell.³³ Research done using a large sized silicon nitride surface did not calculate the reaction of silicon precursors during CVD or ALD processes, only particular properties of silicon nitride such as electron mobility and defect effects were investigated.^{26,27} Although a few silicon precursors, such as SiH_4 , SiH_2Cl_2 and aminosilane were studied, there has been no report on the reactivity of silicon chlorides.

In the present work, we studied the reactivity of different surface sites of β - Si_3N_4 with silicon chlorides using a periodic-slab model of silicon nitride using DFT calculations to understand the underlying reaction mechanism of the ALD process. Three types of surface sites, NH^*/SiH^* , $\text{NH}^*/\text{SiNH}_2^*$, and >Si=N- , were considered. We studied SiCl_4 and Si_2Cl_6 as the silicon precursors to investigate their energies of adsorption and reaction on different surface sites. The reactivity of the different silicon precursors is also discussed. By discovering the influence of surface reaction sites on ALD reactions, we designed a 3-step ALD process sequence to obtain the most effective surface sites for the first half reaction, and confirmed this with deposition experiments.

2. Experimental

2.1. DFT calculations

Our theoretical results presented in this work were obtained by first-principles DFT implemented in the Materials Studio 7.0 with the Dmol³ package (Accelrys, USA).^{35,36} We used the Perdew–Burke–Ernzerhof (PBE) scheme³⁷ in the generalized gradient approximation (GGA) for the exchange correlation functional and the double numerical polarization (DNP) basis set. The scalar relativistic effects were included in the all electron calculation. For more precise results, we chose an octupole scheme for the multipolar expansion. We used smearing of 9×10^{-4} Ha and applied the dipole slab correction in the orbital occupancy scheme. As for geometry optimization, we used a customized quality of convergence tolerance without symmetry constraint until the total energy change was converged to 10^{-6} Ha and all the atomic forces became smaller than 2×10^{-4} Ha \AA^{-1} . Geometry optimizations were performed for all the structures.^{38,39} The van der Waals (vdW) interaction of a precursor molecule with a silicon nitride surface was considered by using the Grimme method.⁴⁰ We compared the local structure, bonds, and formation energies with or without vdW interaction, and the results showed the same trend of reactivities for the different silicon nitride surfaces. Also, the local structure and the bonds were very similar for both cases.

The calculation without the vdW interaction was used in the present study, and the calculation with the vdW interaction is included in the ESI (Fig. S9 and Table S3†). We analysed the electron density and the Fukui indices to visualize the electrophilicity of all atoms of silicon nitride surfaces.

Between the two polymorphic phases of silicon nitride, α -Si₃N₄ and β -Si₃N₄, we chose β -Si₃N₄ to model the silicon nitride surface, because of the metastable structures of α -Si₃N₄ having oxygen defects.^{41–43} The β -Si₃N₄ (001) plane was modeled by the hexagonal lattice of the space group $P6_3/m$ consisting of 6 silicon and 8 nitrogen atoms with the optimized cell parameters of $a = 7.660$ Å and $c = 2.934$ Å, which are in good agreement with those parameters reported in other experimental and theoretical studies.^{44,45} To explore the adsorption properties of the silicon chlorides on the surface, we constructed a 4-layer slab of a (2 × 2) supercell composed of 48 silicon and 64 nitrogen atoms, which has been used to study the reactivity of aminosilane precursors.³³ To avoid interaction from neighbouring slabs, we introduced a vacuum region with a thickness of 20 Å between two adjacent slabs. The slab structure was fully optimized except for the bottom layer which was fixed and passivated with hydrogen atoms to mimic its bulk configuration, as similarly done in other surface calculations.⁴⁶

We constructed three distinct types of silicon nitride top surfaces: (a) a NH*/SiH*-terminated surface, constructed by adding hydrogen atoms to passivate both nitrogen and silicon atoms, containing 160 atoms in total; (b) a NH*/SiNH₂*-terminated surface, transformed from surface (a) by replacing H atoms in Si–H* with NH₂, with a total of 184 atoms; and (c) a bare Si₃N₄ surface, without any modification revealing under-coordinated bare >Si=N– bonds, with total of 136 atoms. We considered SiCl₄ and Si₂Cl₆ molecules as silicon chloride precursors, and each precursor-adsorbed silicon nitride surface was optimized to calculate its adsorption energy E_a using

$$E_a = E_{\text{tot}} - (E_{\text{sur}} + E_{\text{pre}})$$

where E_{tot} , E_{sur} , and E_{pre} are the total energy of the system after adsorption, and the energies of the surface only and the precursor only, respectively, as similarly done for various adsorbates on adsorbents.^{47–53} While considering the different orientations and adsorption sites of a silicon chloride molecule above the surface, we performed geometry optimization for all cases to evaluate their total energies. The case with the lowest adsorption energy was selected as the most stable configuration for adsorption of silicon chloride precursors on the surface.

To search for the reaction path during the ALD process, we performed a transition state (TS) search based on the linear synchronous transit, followed by repeated conjugate gradient minimization and quadratic synchronous transit maximization calculations.^{54–56} The optimized adsorption structure with the lowest energy of adsorption was used as the initial structure for searching the TS. Then, the reaction structure was constructed by forming chemical bonds to simulate the reaction of a precursor molecule with the surface sites. The structure was optimized again, and was used as the final structure in the TS search calculations. TS search calculations enabled us to obtain

the energies of reactions and barriers to determine the kinetic and thermodynamic reactivity of the precursor with the surface.

2.2. ALD of silicon nitride

We used a traveling-wave-type cold-wall reactor equipped with a plasma source. We also used Si₂Cl₆ (UP Chemical Co., Korea) and NH₃ (99.9995%) as the precursor and reactant, respectively. Argon (99.999%) was the purging gas between pulses of precursor and reactant. Silicon nitride films were deposited at 300 °C for 50 cycles. The exposure of Si₂Cl₆ was varied from 1 × 10⁶ L to 5 × 10⁷ L with a fixed NH₃ exposure of 1 × 10⁹ L. For the N₂ plasma steps, capacitively-coupled plasma of 13.56 MHz was used as the source. The rf power, pressure, and time of N₂ plasma were 100 W, 1.5 Torr, and 50 s, respectively. The thickness and refractive index of the deposited films were determined using an ellipsometer (Elli-SE, Ellipso Technology, Korea).

3. Results and discussion

3.1. Structure optimization of surfaces and precursors

β -Si₃N₄ surfaces. We first carried out geometry optimization for all three silicon nitride surface structures described above to obtain the corresponding equilibrium configurations with the lowest total energies.³⁷ Fig. 1 shows the optimized silicon nitride surface structures. There are two kinds of nitrogen atoms at the surfaces of the model. The nitrogen atoms denoted as N_c neighbour with 3 silicon atoms, whereas the nitrogen atoms denoted as N_T neighbour with 2 silicon atoms. According to literature, the bond length of Si–N_c and Si–N_T are 1.743 and 1.748 Å in bulk β -Si₃N₄.^{27,58} In the NH*/SiH*-terminated surface, constructed by adding hydrogen atoms to passivate both nitrogen and silicon atoms, as shown in Fig. 1(a), the bond length of Si–N_c, Si–N_T, N_T–H* and Si–H* are 1.746 Å, 1.731 Å, 1.020 Å and 1.486 Å, respectively. The NH*/SiNH₂*-terminated surface, transformed from Fig. 1(a) by replacing H atoms in Si–H* with NH₂, is shown in Fig. 1(b). The bond length of Si–N_T is slightly reduced to 1.712 Å and the bond length of N_T–H* is slightly increased to 1.041 Å as compared with the first surface structure shown in Fig. 1(a). The new bonds of Si–NH₂* and N–H₂* are 1.771 Å and 1.023 Å, respectively. The bond lengths of Si–N_c and Si=N_T of the under-coordinated bare >Si=N– surface in Fig. 1(c) are 1.743 and 1.750 Å, respectively, which are in good agreement with the bulk bond lengths in the literature.³⁰ Fig. 1(c) also shows the double bonds between Si and N_T at the surface.

Silicon chloride precursors. The optimized structures of SiCl₄ and Si₂Cl₆ including the bond lengths and bond angles are shown in Table 1. The calculated Si–Cl bond lengths are 2.042 Å and 2.053 Å in SiCl₄ and Si₂Cl₆, respectively, which are in good agreement with the literature.^{59–61} In Si₂Cl₆, the length of the Si–Si bond is 2.345 Å, which is 0.292 Å longer than that of the Si–Cl bond.

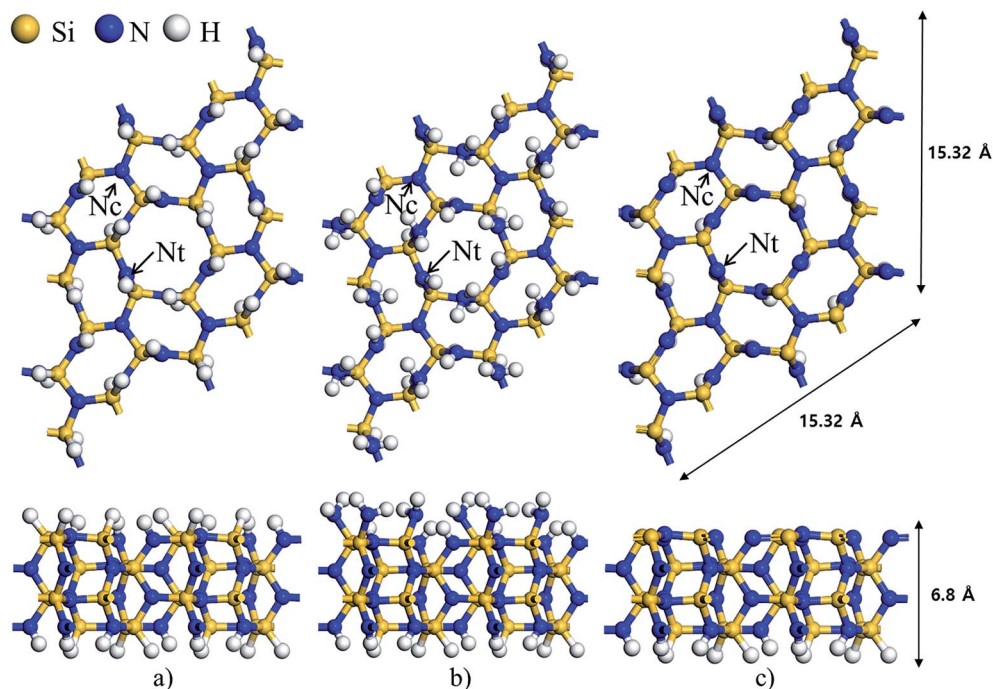
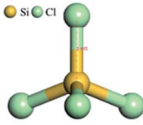
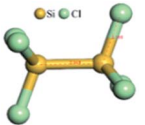


Fig. 1 The optimized β - Si_3N_4 surface structures with (a) NH^*/SiH^* , (b) $\text{NH}^*/\text{SiNH}_2^*$, and (c) $>\text{Si}=\text{N}$ - termination. The nitrogen atoms denoted as N_c neighbour with 3 silicon atoms, whereas the nitrogen atoms denoted as N_T neighbour with 2 silicon atoms at the surface. Top and bottom figures correspond to the plan view and the cross-sectional view of the silicon nitride models of this study.

Table 1 Bond lengths and bond angles of the optimized structures of SiCl_4 and Si_2Cl_6 molecules

Precursors				
Length (Å)	Si-Cl	2.042	Si-Cl	2.053
			Si-Si	2.345
Angle (°)	Cl-Si-Cl	109.5	Cl-Si-Cl	109.63
			Cl-Si-Si	109.27

3.2. Adsorption and reaction on the NH^*/SiH^* -terminated β - Si_3N_4 surface

SiCl_4 precursor. We considered two orientations and four positions of SiCl_4 above the surface. The details of all eight cases are shown in the ESI (Fig. S1†).

Fig. 2 shows the optimized structures for adsorption and reaction of SiCl_4 on the NH^*/SiH^* -terminated β - Si_3N_4 surfaces.

The optimized structure of the system with the lowest adsorption energy of SiCl_4 on the surface is shown in Fig. 2(a). In Fig. 2(c), a chlorine atom from SiCl_4 reacts with the hydrogen atom of $\text{N}_T\text{-H}^*$ to form HCl, while the remaining atoms of SiCl_4 react with the surface to form $\text{N}_T\text{-SiCl}_3^*$. The lowest adsorption energy is -0.04 eV, indicating that the adsorption is energetically favorable. However, the energy of reaction is 0.78 eV, which

shows that the reaction is endothermic. The energy barrier from Fig. 2(a)–(c) is 4.99 eV with the transition state structure shown in Fig. 2(b). The distances between Si (precursor) and N (surface) during adsorption and transition state were 6.04 Å and 4.54 Å, respectively, with no obvious surface reconstruction during the reaction. These results indicate that it is difficult for SiCl_4 to react with the NH^*/SiH^* -terminated surfaces.

Si_2Cl_6 precursor. The procedure used for obtaining the optimized structures for adsorption (Fig. S2†) and reaction of SiCl_4 was also implemented for Si_2Cl_6 precursors. Fig. 3 shows the optimized structure for adsorption, transition state, and reaction of Si_2Cl_6 on the NH^*/SiH^* -terminated surface. The reaction of Si_2Cl_6 with the surface also produces HCl as the byproduct and newly formed $\text{N}_T\text{-Si}_2\text{Cl}_5^*$ on the surface as shown in Fig. 3(c). Its lowest adsorption energy is -0.04 eV similar to the SiCl_4 case.

Both SiCl_4 and Si_2Cl_6 on the NH^*/SiH^* -terminated surface have an endothermic energy of reaction. The energy of reaction of Si_2Cl_6 is 0.84 eV with an energy barrier of 5.32 eV, which are higher than those of SiCl_4 . The distances between Si (precursor) and N (surface) during adsorption and transition state were 5.25 Å and 3.60 Å, respectively, also with no obvious surface reconstruction appearing during the reaction. It is also difficult for Si_2Cl_6 to react with the NH^*/SiH^* -terminated surfaces.

3.3. Adsorption and reaction on the $\text{NH}^*/\text{SiNH}_2^*$ -terminated β - Si_3N_4 surface

SiCl_4 precursor. The adsorption and reaction of SiCl_4 on the $\text{NH}^*/\text{SiNH}_2^*$ -terminated surface are shown in Fig. 4(a) and (c),

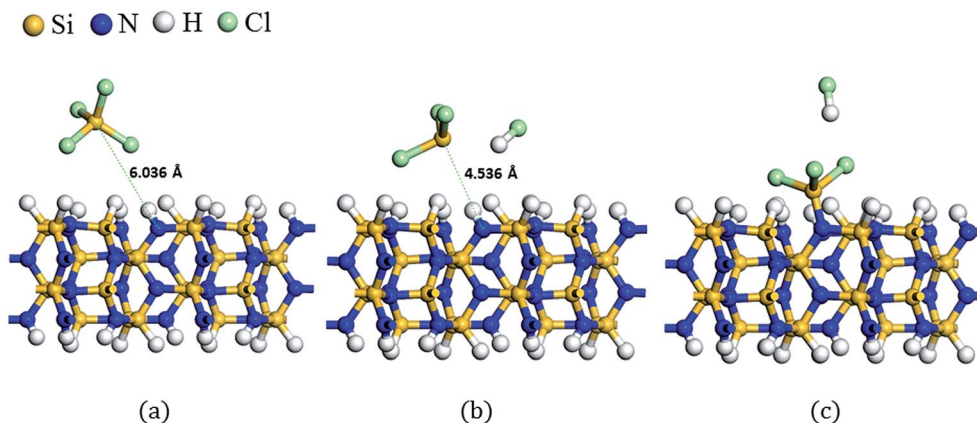


Fig. 2 The optimized structures for (a) adsorption, (b) transition state and (c) reaction of a SiCl_4 molecule on the NH^*/SiH^* -terminated $\beta\text{-Si}_3\text{N}_4$ surface.

with a transition state shown in Fig. 4(b). In Fig. 4(c), SiCl_4 reacts with Si-NH_2^* to form Si-NH-SiCl_3^* and HCl . A chlorine atom dissociated from SiCl_4 reacts with a hydrogen atom dissociated from the Si-NH_2^* to form HCl above the surface. The lowest energies of adsorption and reaction are -0.05 eV and -1.12 eV, which indicates that both the adsorption and reaction are exothermic. We obtained an energy barrier of 4.89 eV, which is slightly lower than the energy barrier of SiCl_4 on the NH^*/SiH^* -terminated surface. The distances between Si (precursor) and N (surface) during adsorption and transition state were 4.38 Å and 3.16 Å, respectively, with a slight surface reconstruction during the reaction. It was found that hydrogen atoms located below the precursor on the surface seem to be shifted a little bit during the transition state with respect to the corresponding initial structure.

Si_2Cl_6 precursor. The adsorption and reaction of Si_2Cl_6 on the $\text{NH}^*/\text{SiNH}_2^*$ -terminated surface is shown in Fig. 5(a) and (c), with a transition state shown in Fig. 5(b). Fig. 5(c) shows newly formed $\text{Si-NH-Si}_2\text{Cl}_5^*$ and HCl . A hydrogen atom dissociated from the Si-NH_2^* also reacts with a dissociated chlorine

to form HCl above the neighbouring Si-NH_2^* surface, which shows the same tendency as the reaction of SiCl_4 . The lowest energies of adsorption and reaction are -0.04 eV and -1.14 eV with an energy barrier of 3.55 eV. The distances between Si (precursor) and N (surface) during adsorption and transition state were 5.08 Å and 3.46 Å, respectively, which also exhibit a slight surface reconstruction during the transition state, as observed similarly in the SiCl_4 case.

3.4. Adsorption and reaction on the under-coordinated bare $\text{Si}=\text{N}-\beta\text{-Si}_3\text{N}_4$ surface

SiCl_4 precursor. The optimized structures for the adsorption, transition state, and reaction of SiCl_4 on the under-coordinated bare $\text{Si}=\text{N}_\text{T}$ surface are shown in Fig. 6. Fig. 6(c) shows that the silicon atom in SiCl_4 reacts with an N_T to form a 5-coordinate structure and that the double bond of $\text{Si}=\text{N}_\text{T}$ before the reaction is transformed to single bond of $\text{Si}-\text{N}_\text{T}$ by the reaction. The lowest energies for adsorption and reaction are -0.15 eV and -1.92 eV with a very low energy barrier of 0.05 eV. The distances between Si (precursor) and N (surface) during

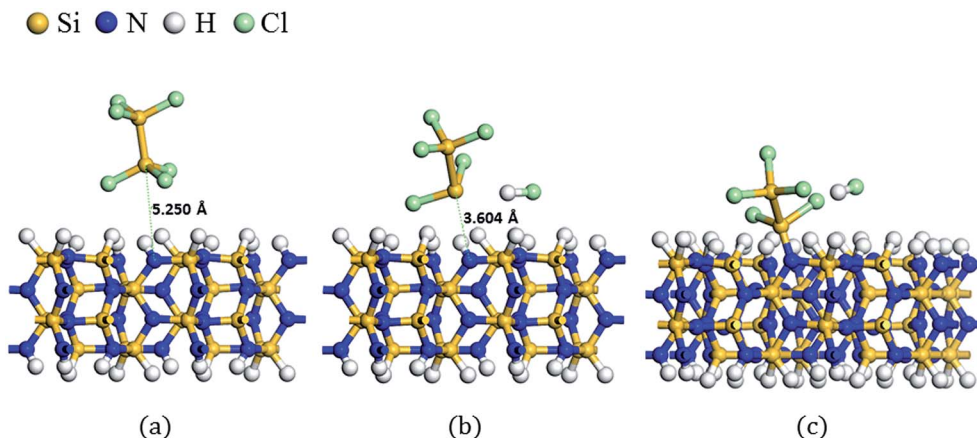


Fig. 3 The optimized structures for (a) adsorption, (b) transition state and (c) reaction of a Si_2Cl_6 molecule on the NH^*/SiH^* -terminated $\beta\text{-Si}_3\text{N}_4$ surface.

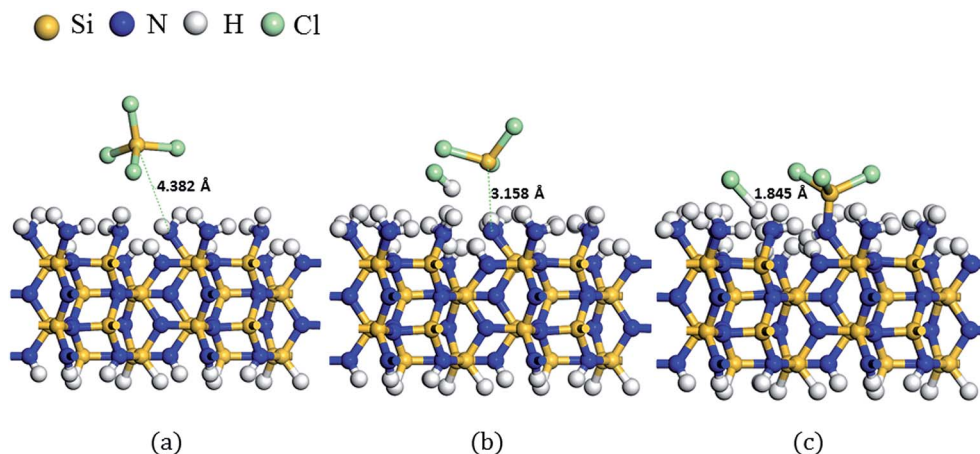


Fig. 4 The optimized structures for (a) adsorption, (b) transition state and (c) reaction of a SiCl_4 molecule on the $\text{NH}^*/\text{SiNH}_2^*$ -terminated $\beta\text{-Si}_3\text{N}_4$ surface.

adsorption and transition state were 3.39 Å and 2.80 Å, respectively, with no obvious surface reconstruction observed.

Si_2Cl_6 precursor. The optimized structures for the adsorption, transition state, and reaction of Si_2Cl_6 on the under-coordinated bare (>Si=N-) surface are shown in Fig. 7. Fig. 7(c) shows that the silicon atom in Si_2Cl_6 reacts with an N_T atom and that a chlorine atom dissociated from the precursor reacts with a silicon atom on the surface. Also, the double bond of $\text{Si}=\text{N}_\text{T}$ is transformed to the single bond of $\text{Si}-\text{N}_\text{T}$ by the reaction. The lowest energies for adsorption and reaction are -0.02 eV and -2.39 eV with a very low energy barrier of 0.193 eV. The distances between Si (precursor) and N (surface) during adsorption and transition state were 4.75 Å and 2.86 Å, respectively, also with no obvious surface reconstruction appearing during the reaction.

3.5. Discussion

To summarize the calculation results, the energy diagrams for all of the reactions of silicon chlorides with different kinds of

surfaces are shown in Fig. 8. The detailed structures of $\beta\text{-Si}_3\text{N}_4$ surfaces for transition state calculations can be found in the ESI (Fig. S3–S8†).

During the adsorption of the precursors on the $\beta\text{-Si}_3\text{N}_4$ surfaces, both SiCl_4 and Si_2Cl_6 precursors show weak exothermic adsorption energies ranging from -0.02 eV to -0.15 eV, which correspond to the energy values of a hydrogen bond (0.03–0.3 eV) between hydrogen and chlorine atoms^{62–64} or van der Waals forces (0.01–1 eV).⁶⁵

Both precursors react with $\text{N}_\text{T}-\text{H}^*$ rather than $\text{Si}-\text{H}^*$, because the bond strength of Si–N is higher than the Si–Si bond.⁶⁶ SiCl_4 tends to form shorter Si–N bonds on the $\beta\text{-Si}_3\text{N}_4$ surface than Si_2Cl_6 does, regardless of the reaction stages. Such a trend may occur due to the differences in electronegativity of the silicon atoms between the two precursors. A Si atom in SiCl_4 has one less electron than that in Si_2Cl_6 , which means the free electron pair from nitrogen on the surface will attract SiCl_4 stronger than Si_2Cl_6 .

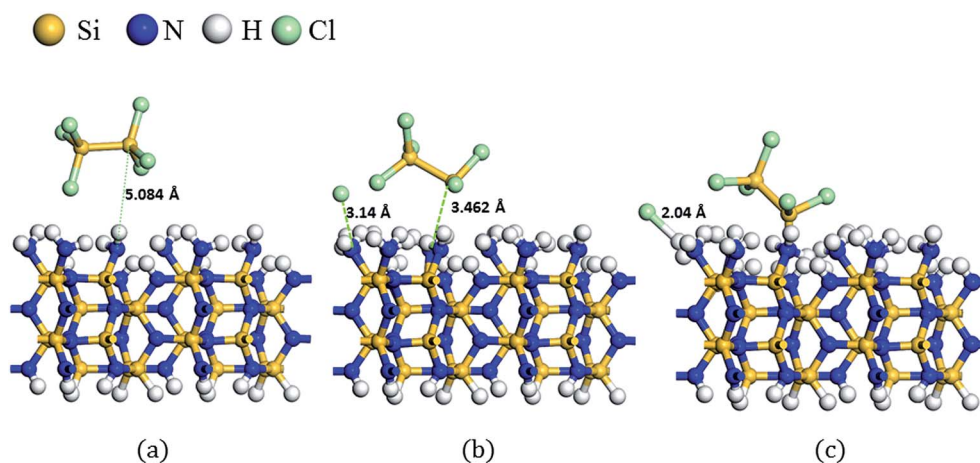


Fig. 5 The optimized structures for (a) adsorption, (b) transition state and (c) reaction of a Si_2Cl_6 molecule on the $\text{NH}^*/\text{SiNH}_2^*$ -terminated $\beta\text{-Si}_3\text{N}_4$ surface.

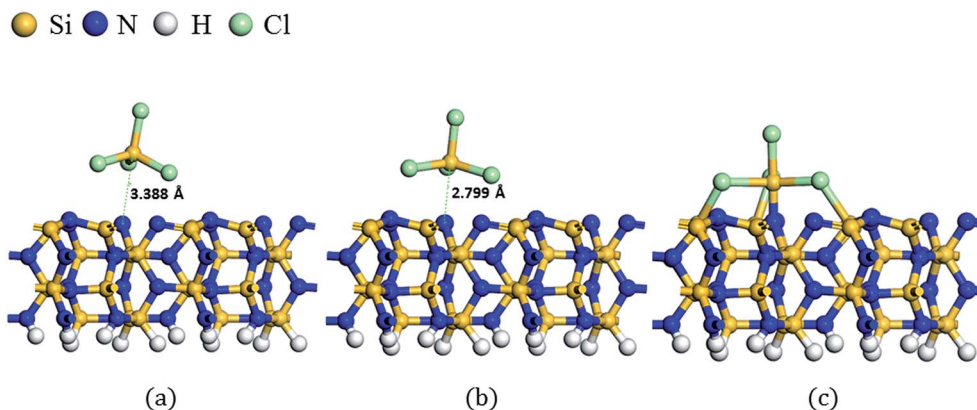


Fig. 6 The optimized structures for (a) adsorption, (b) transition state and (c) reaction of a SiCl_4 molecule on the under-coordinated bare >Si=N- $\beta\text{-Si}_3\text{N}_4$ surface.

On the NH^*/SiH^* -terminated surfaces, the reactions of precursors on the NH^*/SiH^* -terminated surfaces show positive energy values, indicating that the reaction is not energetically favorable. The energy barriers of 4.99 eV and 5.32 eV correspond to the bond dissociation energy of hydrogen from $\text{N}_\text{T}\text{-H}^*$ (~ 4.81 eV).⁶⁷

Contrarily, exothermic reactions were obtained for both precursors on the $\text{NH}^*/\text{SiNH}_2^*$ -terminated surface. While silicon precursors react with $\text{N}_\text{T}\text{-H}^*$ sites on the NH^*/SiH^* -terminated surfaces, silicon precursors react with Si-NH_2^* on the $\text{NH}^*/\text{SiNH}_2^*$ -terminated surface due to the higher position with less steric hindrance of the Si-NH_2^* surface site as compared with the $\text{N}_\text{T}\text{-H}^*$ sites. For SiCl_4 , the energy barrier of 4.89 eV is almost the same as that on the NH^*/SiH^* -terminated surface, because the dissociation of hydrogen and the formation of an HCl molecule during the transition state in Fig. 4(b) are very similar to the transition state on the NH^*/SiH^* -terminated surface in Fig. 3(b). For Si_2Cl_6 , however, the energy barrier is lower than that on the NH^*/SiH^* -terminated surface because

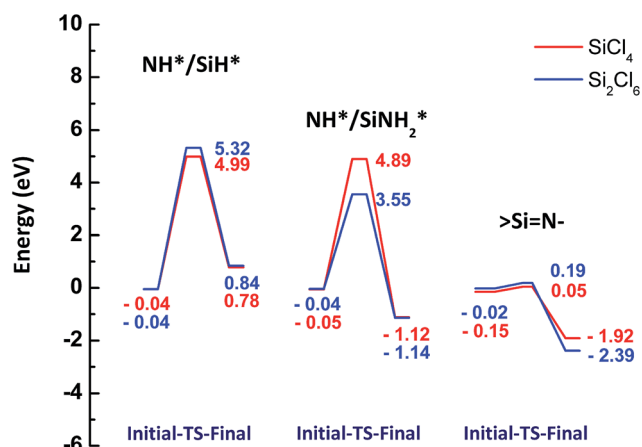


Fig. 8 Energy diagram of SiCl_4 and Si_2Cl_6 on the NH^*/SiH^* -terminated, the $\text{NH}^*/\text{SiNH}_2^*$ -terminated, and the under-coordinated bare >Si=N- $\beta\text{-Si}_3\text{N}_4$ surfaces.

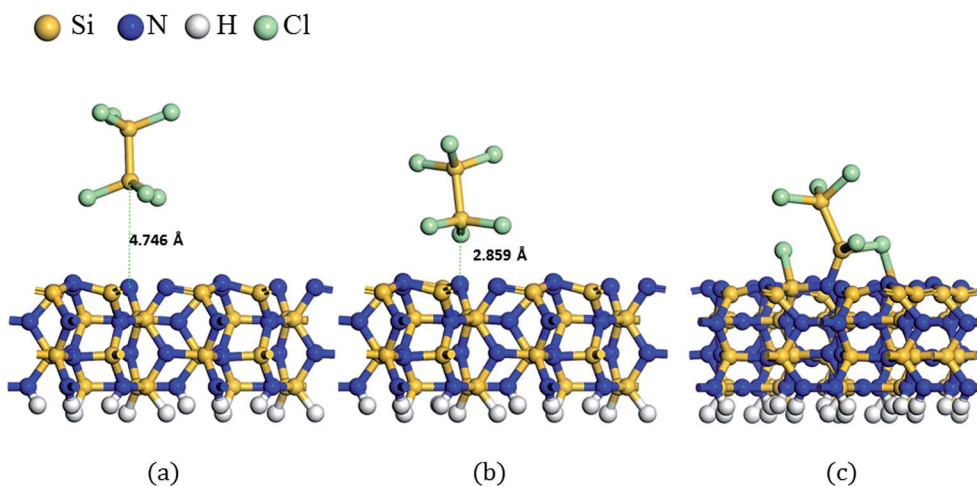


Fig. 7 The optimized structures for (a) adsorption, (b) transition state and (c) reaction of a Si_2Cl_6 molecule on the under-coordinated bare >Si=N- $\beta\text{-Si}_3\text{N}_4$ surface.

of the difference in the transition state structure shown in Fig. 5(b). The optimized transition state structure only shows the dissociation of a chlorine atom from the precursor without the dissociation of a hydrogen atom from the surface. The energy barrier of 3.55 eV corresponds to the bond dissociation energy of Si–Cl (3.9–4.3 eV),^{66,68} which is lower than the bond dissociation energy of N_T–H. The lower energy barrier for the reaction of Si₂Cl₆ with the NH*/SiNH₂*-terminated surface agrees well with the lower saturation dose of 2×10^8 L (ref. 16) of Si₂Cl₆ as compared with 2×10^{10} L (ref. 14) of SiCl₄ for the ALD of silicon nitride using NH₃ as the reactant.

Meanwhile, the reactions of both precursors on the under-coordinated bare >Si=N– surface are energetically most favorable with very low energy barriers. The presence of unsaturated double bonds between nitrogen and silicon atoms (>Si=N–) makes the under-coordinated bare surface the most reactive surface. One of the theoretical studies suggested that the under-coordinated bare β-Si₃N₄ surface without saturation of the hydrogen atoms is energetically unstable, resulting in very reactive surfaces.³⁰ The silicon atom from the precursors easily reacts with the unsaturated N_T atom on the surface, and chlorine atoms of the precursors also easily react with unsaturated silicon atoms on the surface.

We analysed the electron density and the Fukui indices to visualize the electrophilicity of all atoms of different silicon nitride surfaces (Fig. 9). This analysis also supports the trend reactivities of different surfaces expected by formation energies. The red colour indicates greater values of electrophilicity, and the blue colour indicates lower values of electrophilicity. Generally, a precursor molecule tends to react with the atom which has a greater value of electrophilicity.³³ In the NH*/SiH* surface, the charge was evenly spread. In the NH*/SiNH₂* surface, however, the SiNH₂* sites have a higher value than that of the NH* sites. For the –Si=N– case, the electrophilicity value of the Si=N sites was the highest among the three kinds of surfaces with a bright yellow colour, which means that the Si=N sites are most reactive to the precursor molecules.

Silicon nitride films produced by ALD or CVD are amorphous and saturated by hydrogen atoms. If we assume that the surface of amorphous silicon nitride films consists of the different types of surface sites modeled in this study, the under-coordinated

bare surface site will react fastest with the silicon precursors. Then, the chlorine atom dissociated from the silicon precursors would react with the neighbouring hydrogen to form unsaturated nitrogen and hydrogen atoms on the surface, because atomic chlorine is more reactive than the silicon precursors. Therefore, the reaction of the precursors would propagate to the neighbouring surface sites. However, the dissociation of the strongly-bound hydrogen on the surface by atomic chlorine also would have a high energy barrier, which makes the deposition process very slow.

N₂ plasma produces an under-coordinated surface which is the most reactive surface for silicon chlorides, however, no film is grown by alternating exposure to Si₂Cl₆ and N₂ plasma, because chlorine is not reactive with nitrogen in the second half reaction of the ALD process. NH₃ or NH₃ plasma react with chlorine on the surface to cause the second half reaction, however, they produce a NH*/SiNH₂*-terminated surface which is less reactive with silicon chlorides during the first half reaction. To enhance the first half reaction of the ALD by alternating exposures to a silicon chloride and NH₃, a high density of the under-coordinated surface sites is desirable. Therefore, we designed a 3-step ALD process sequence by adding an additional N₂ plasma step in every ALD cycle prior to the introduction of the silicon chloride precursor.

3.6. Effect of surface plasma treatment on thermal ALD of silicon nitride

Fig. 10 compares a 3-step ALD process with the conventional 2-step ALD process. For both ALD processes, the saturation dose and the saturated growth rate were measured by changing the exposures of Si₂Cl₆ precursors. Fig. 11 shows the thickness of the deposited film as a function of Si₂Cl₆ precursors with or without N₂ plasma steps.

The 3-step process showed higher growth rates as compared with the 2-step process. In the 2-step ALD without the N₂ plasma steps, the growth rates increased from 0.34 to 0.59 Å per cycle as the Si₂Cl₆ exposures increases from 10⁶ to 10⁷ L. With the N₂ plasma steps, the growth rates were 1.1 Å per cycle, which is almost twice that of the 2-step case. Also, the saturation dose of the Si₂Cl₆ precursor was reduced from 10⁷ L or higher to 1×10^6 L by adding N₂ plasma steps. Therefore, it was proven that the

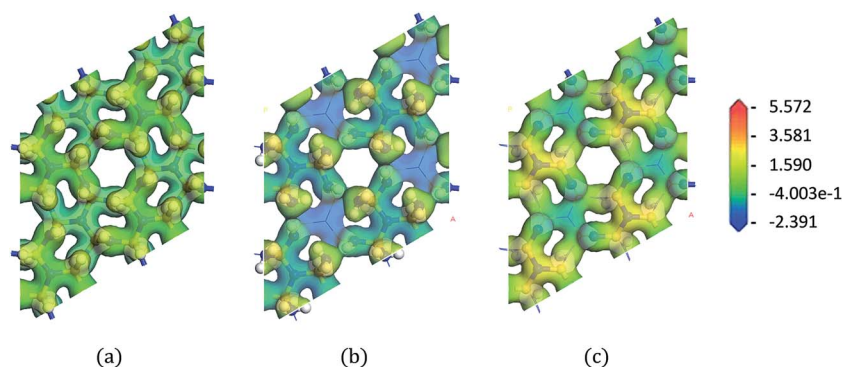


Fig. 9 The electron density of (a) NH*/SiH*, (b) NH*/SiNH₂*, and (c) >Si=N– termination, using Fukui indices for electrophilicity.

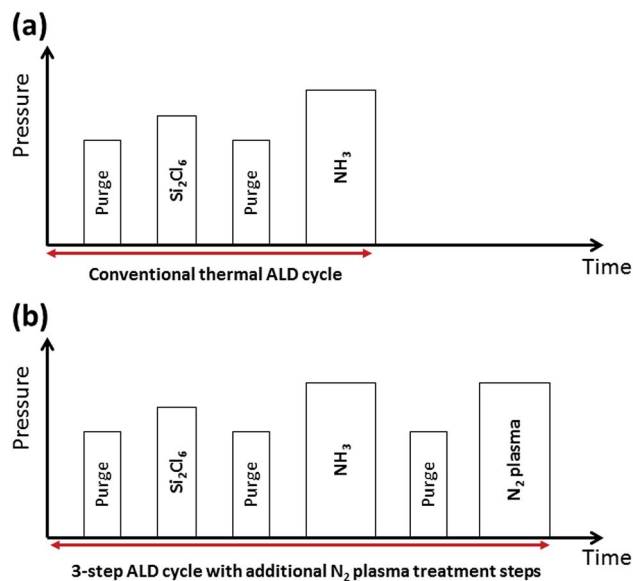


Fig. 10 ALD process sequences: (a) the 2-step ALD using Si_2Cl_6 and NH_3 , and (b) the 3-step ALD with additional N_2 plasma steps.

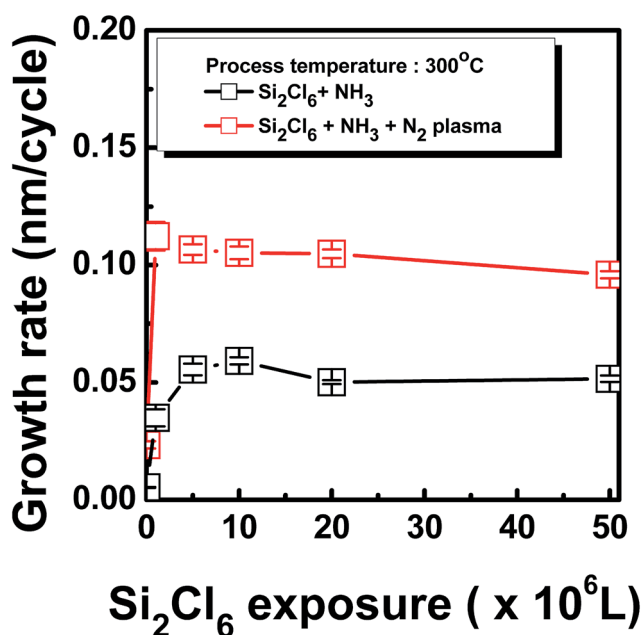


Fig. 11 The thickness of the silicon nitride films prepared by thermal ALD with or without N_2 plasma treatments. The film was deposited by alternating exposures to Si_2Cl_6 and NH_3 at 300°C for 50 cycles.

N_2 plasma enhances the deposition reaction of the thermal ALD of silicon nitride using silicon chloride and NH_3 .

4. Conclusions

The reactions of SiCl_4 and Si_2Cl_6 with three types of $\beta\text{-Si}_3\text{N}_4$ surface sites were studied using DFT calculations. The reactions of the silicon precursors with the $\text{NH}^*/\text{SiNH}_2^*$ -terminated surface and the under-coordinated bare >Si=N- surface are

energetically favorable, whereas the reactions are endothermic with the NH^*/SiH^* -terminated surface. On the under-coordinated surface, the silicon atom and the chlorine atoms of the precursors easily react with unsaturated N_T atoms and unsaturated silicon atoms, respectively, resulting in very low energy barriers for the reaction. However, the NH^*/SiH^* - and $\text{NH}^*/\text{SiNH}_2^*$ -terminated surfaces showed high energy barriers corresponding to the dissociation of a hydrogen atom from the surface or a chlorine atom from the precursor. Si_2Cl_6 shows lower energies of reaction as compared with those of SiCl_4 on the under-coordinated surface. From the understanding of the influence of the surface on the deposition reaction, N_2 plasma steps were added into every cycle prior to the introduction of silicon precursors in order to transform the Si-NH_2^* surface sites to under-coordinated bare >Si=N- sites. The saturation dose was reduced from 10^7 L to $<10^6$ L and the growth per cycle was increased from 0.59 \AA per cycle to 1.1 \AA per cycle by the additional N_2 plasma steps, which is in good agreement with our calculations. These results show that the reactivity of the surface sites plays a very important role to determine the thermodynamics and kinetics of ALD processes.

Acknowledgements

W.-J. L. would like to acknowledge financial support from the Industrial Strategic Technology Development Program (Project No. 10041792) funded by MOTIE (Ministry of Trade, Industry & Energy). Y.-K. K. would like to acknowledge financial support from the Future Semiconductor Device Technology Development Program (Project No. 10045360) funded by MOTIE (Ministry of Trade, Industry & Energy) and KSRC (Korea Semiconductor Research Consortium).

References

- 1 K. J. Yang, T.-J. King, C. Hu, S. Levy and H. N. Al-Shareef, *Solid-State Electron.*, 2003, **47**, 149–153.
- 2 A. Bahari, F. Pourzaman and M. Hoseni, *Int. J. Phys. Sci.*, 2011, **6**, 1146–1151.
- 3 A. Nakajima, Q. D. M. Khosru, T. Yoshimoto, T. Kidera and S. Yokoyama, *J. Vac. Sci. Technol., B*, 2002, **20**, 1406–1409.
- 4 N. Sharma, M. Hooda and S. K. Sharma, *J. Mater.*, 2014, **2014**, 1–8.
- 5 B. C. Joshi, G. Eranna, D. P. Runthala, B. B. Dixit, O. P. Wadhawan and P. D. Yyas, *Indian J. Eng. Mater. Sci.*, 2000, **7**, 303–309.
- 6 W. M. Arnoldbik, C. H. M. Marée, A. J. H. Maas, M. J. van den Boogaard, F. H. P. M. Habraken and A. E. T. Kuiper, *Phys. Rev. B*, 1993, **48**, 5444–5456.
- 7 W. Huang, X. Wang, M. Sheng, L. Xu, F. Stubhan, L. Luo, T. Feng, X. Wang, F. Zhang and S. Zou, *Mater. Sci. Eng., B*, 2003, **98**, 248–254.
- 8 A. El Amrani, A. Bekhtari, B. Mahmoudi, A. Lefgoum and H. Menari, *Vacuum*, 2011, **86**, 386–390.
- 9 L. Zamboni, *Vacuum*, 2003, **71**, 439–444.
- 10 A. Kshirsagar, P. Nyaupane, D. Bodas, S. P. Duttgupta and S. A. Gangal, *Appl. Surf. Sci.*, 2011, **257**, 5052–5058.

- 11 H. Zhou, K. Elgaid, C. Wilkinson and I. Thayne, *Jpn. J. Appl. Phys.*, 2006, **45**, 8388–8392.
- 12 K. Suemitsu, Y. Kawano, H. Utsumi, H. Honjo, R. Nebashi, S. Saito, N. Ohshima, T. Sugibayashi, H. Hada, T. Nohisa, T. Shimazu, M. Inoue and N. Kasai, *Jpn. J. Appl. Phys.*, 2008, **47**, 2714–2718.
- 13 W.-J. Lee, J.-H. Lee, C. O. Park, Y.-S. Lee, S.-J. Shin and S.-K. Rha, *J. Korean Phys. Soc.*, 2004, **45**, 1352–1355.
- 14 J. W. Klaus, A. W. Ott, A. C. Dillon and S. M. George, *Surf. Sci.*, 1998, **418**, L14–L19.
- 15 W.-J. Lee, U.-J. Kim, C.-H. Han, M.-H. Chun, S.-K. Rha and Y.-S. Lee, *J. Korean Phys. Soc.*, 2005, **47**, S598–S602.
- 16 K. Park, W.-D. Yun, B.-J. Choi, H.-D. Kim, W.-J. Lee, S.-K. Rha and C. O. Park, *Thin Solid Films*, 2009, **517**, 3975–3978.
- 17 F. Koehler, D. H. Triyoso, I. Hussain, S. Mutas and H. Bernhardt, *IOP Conf. Ser.: Mater. Sci. Eng.*, 2012, **41**, 012006.
- 18 D. H. Triyoso, K. Hempel, S. Ohsiek, V. Jaschke, J. Shu, S. Mutas, K. Dittmar, J. Schaeffer, D. Utesch and M. Lenski, *ECS J. Solid State Sci. Technol.*, 2013, **2**, N222–N227.
- 19 W. Choi, H. Ryu, N. Jeon, M. Lee, H.-Y. Cha and K.-S. Seo, *IEEE Electron Device Lett.*, 2014, **35**, 30–32.
- 20 S. W. King, *J. Vac. Sci. Technol., A*, 2011, **29**, 041501.
- 21 F. L. Riley, *J. Am. Ceram. Soc.*, 2000, **83**, 245–265.
- 22 S. Morishita, S. Sugahara and M. Matsumura, *Appl. Surf. Sci.*, 1997, **112**, 198–204.
- 23 H. Goto, K. Shibahara and S. Yokoyama, *Appl. Phys. Lett.*, 1996, **68**, 3257.
- 24 D. Kim, D. Kim, H. Kim, H. So and M. Hong, *Curr. Appl. Phys.*, 2011, **11**, S67–S72.
- 25 K. Jarolimek, R. A. de Groot, G. A. de Wijs and M. Zeman, *Phys. Rev. B*, 2010, **82**, 205201.
- 26 L. E. Hintzsche, C. M. Fang, T. Watts, M. Marsman, G. Jordan, M. W. P. E. Lamers, A. W. Weeber and G. Kresse, *Phys. Rev. B*, 2012, **86**, 235204.
- 27 M.-E. Grillo, S. D. Elliott and C. Freysoldt, *Phys. Rev. B*, 2011, **83**, 085208.
- 28 T. A. Pham, T. Li, S. Shankar, F. Gygi and G. Galli, *Phys. Rev. B*, 2011, **84**, 045308.
- 29 A. A. Korkin, J. V. Cole, D. Sengupta and J. B. Adams, *J. Electrochem. Soc.*, 1999, **146**, 4203–4212.
- 30 A. A. Bagatur'yants, K. P. Novoselov, A. A. Safonov, J. V. Cole, M. Stoker and A. A. Korkin, *Surf. Sci.*, 2001, **486**, 213–225.
- 31 C. Mui, Y. Widjaja, J. K. Kang and C. B. Musgrave, *Surf. Sci.*, 2004, **557**, 159–170.
- 32 C. A. Murray, S. D. Elliott, D. Hausmann, J. Henri and A. LaVoie, *ACS Appl. Mater. Interfaces*, 2014, **6**, 10534–10541.
- 33 L. Huang, B. Han, B. Han, A. Derecskei-Kovacs, M. Xiao, X. Lei, M. L. O'Neill, R. M. Pearlstein, H. Chandra and H. Cheng, *Phys. Chem. Chem. Phys.*, 2014, **16**, 18501.
- 34 F. Filippone, *J. Phys.: Condens. Matter*, 2014, **26**, 395009.
- 35 B. Delley, *J. Chem. Phys.*, 1990, **92**, 508–517.
- 36 B. Delley, *J. Chem. Phys.*, 2000, **113**, 7756–7764.
- 37 J. P. Perdew, K. Burke and M. Ernzerhof, *Phys. Rev. Lett.*, 1996, **77**, 3865–3868.
- 38 J. Baker, A. Kessi and B. Delley, *J. Chem. Phys.*, 1996, **105**, 192–212.
- 39 J. Andzelm, R. D. King-Smith and G. Fitzgerald, *Chem. Phys. Lett.*, 2001, **335**, 321–326.
- 40 E. R. McNellis, J. Meyer and K. Reuter, *Phys. Rev. B*, 2009, **80**, 205414.
- 41 J. Melendezmartinez, *Prog. Mater. Sci.*, 2004, **49**, 19–107.
- 42 O. N. Carlson, *Bull. Alloy Phase Diagrams*, 1990, **11**, 569–573.
- 43 R. P. Vedula, N. L. Anderson and A. Strachan, *Phys. Rev. B*, 2012, **85**, 205209.
- 44 R. Belkada, M. Kohyama, T. Shibayanagi and M. Naka, *Phys. Rev. B*, 2002, **65**, 092104.
- 45 R. Belkada, T. Shibayanagi and M. Naka, *J. Am. Ceram. Soc.*, 2000, **83**, 2449–2454.
- 46 H. Oh, Y. J. Hong, K.-S. Kim, S. Yoon, H. Baek, S.-H. Kang, Y.-K. Kwon, M. Kim and G.-C. Yi, *NPG Asia Mater.*, 2014, **6**, e145.
- 47 S. Woo and Y.-K. Kwon, *Phys. Rev. B*, 2009, **79**, 075404.
- 48 K. Young-Kyun, *J. Korean Phys. Soc.*, 2010, **57**, 778–786.
- 49 S. H. Kang, G. Kim and Y. K. Kwon, *J. Phys.: Condens. Matter*, 2011, **23**, 505301.
- 50 G. Kim, S.-H. Kang, C.-y. Lim and Y.-K. Kwon, *Chem. Phys. Lett.*, 2012, **545**, 83–87.
- 51 H.-J. Lee, G. Kim and Y.-K. Kwon, *Chem. Phys. Lett.*, 2013, **580**, 57–61.
- 52 H. Y. Jung, Y. L. Kim, S. Park, A. Datar, H. J. Lee, J. Huang, S. Somu, A. Busnaina, Y. J. Jung and Y. K. Kwon, *Analyst*, 2013, **138**, 7206–7211.
- 53 S.-Y. Won, J.-H. Kim, H. Kim, J. K. Yoon, S.-J. Kahng, Y.-K. Kwon and Y. Park, *J. Phys. Chem. C*, 2013, **117**, 21371–21375.
- 54 J. Baker, *J. Comput. Chem.*, 1985, **7**, 385–395.
- 55 N. Govind, M. Petersen, G. Fitzgerald, D. King-Smith and J. Andzelm, *Comput. Mater. Sci.*, 2003, **28**, 250–258.
- 56 C. J. Cerjan, *J. Chem. Phys.*, 1981, **75**, 2800–2806.
- 57 M. Weinert and J. W. Davenport, *Phys. Rev. B*, 1992, **45**, 13709–13712.
- 58 V. M. Bermudez, *Surf. Sci.*, 2005, **579**, 11–20.
- 59 J. M. Wittbrodt and H. B. Schlegel, *Chem. Phys. Lett.*, 1997, **265**, 527–531.
- 60 J. A. Tossell, *Surf. Sci.*, 1999, **431**, 186–192.
- 61 S. P. Chan, Z. F. Liu, W. M. Lau and J. S. Tse, *Surf. Sci.*, 1999, **432**, 125–138.
- 62 L. Arnadottir, E. M. Stuve and H. Jonsson, *Surf. Sci.*, 2010, **604**, 1978–1986.
- 63 J. Fraxedas, *Molecular Organic Materials: From Molecules to Crystalline Solids*, Cambridge University Press, New York, USA, 2006.
- 64 A. Mardyukov, Dissertation, Ruhr-Universität Bochum, 2010.
- 65 J. W. McPherson, *Reliability Physics and Engineering: Time-To-Failure Modeling*, Springer International Publishing, Switzerland, 2013.
- 66 Y.-R. Luo, *Handbook of Bond Dissociation Energies in Organic Compounds*, CRC Press, Boca Raton, Florida, 2002.
- 67 R. Walsh, *Bond Dissociation Energies in Organosilicon Compounds*, <http://www.gelest.com/goods/pdf/library/10bonddiss.pdf>, (accessed May 2015).
- 68 R. W. Fahs II and M. D. W. Fahs, *US Pat.*, US20130056648A1, 2013.